

# Feature Flow Regularization: Improving Structured Sparsity in Deep Neural Networks

**Yue Wu**

Department of Mathematics  
HKUST  
ywudb@connect.ust.hk

**Yuan Lan**

Department of Mathematics  
HKUST  
ylanaa@connect.ust.hk

**Luchan Zhang**

Department of Mathematics  
HKUST  
malczhang@ust.hk

**Yang Xiang**

Department of Mathematics  
HKUST  
maxiang@ust.hk

## Abstract

Pruning is a model compression method that removes redundant parameters in deep neural networks (DNNs) while maintaining accuracy. Most available filter pruning methods require complex treatments such as iterative pruning, features statistics/ranking, or additional optimization designs in the training process. In this paper, we propose a simple and effective regularization strategy from a new perspective of evolution of features, which we call feature flow regularization (FFR), for improving structured sparsity and filter pruning in DNNs. Specifically, FFR imposes controls on the gradient and curvature of feature flow along the neural network, which implicitly increases the sparsity of the parameters. The principle behind FFR is that coherent and smooth evolution of features will lead to an efficient network that avoids redundant parameters. The high structured sparsity obtained from FFR enables us to prune filters effectively. Experiments with VGGNets, ResNets on CIFAR-10/100, and Tiny ImageNet datasets demonstrate that FFR can significantly improve both unstructured and structured sparsity. Our pruning results in terms of reduction of parameters and FLOPs are comparable to or even better than those of state-of-the-art pruning methods.

## 1 Introduction

Deep neural networks (DNNs) have achieved huge success in a wide range of applications. Meanwhile, DNNs require considerably more computational cost and storage space as they become deeper in order to achieve higher accuracy. Deeper models generally contain more redundant weights [4]. Several model compression methods are proposed to balance accuracy and model complexity, e.g. weight pruning [18, 9, 8, 7] and quantization [6], low-rank approximation [5, 16, 3], and sparsity structure learning [26, 2, 23]. Weight pruning removes less important weights in the network while maintaining accuracy. In particular, filter pruning [20] removes weights at the level of filters, which can compress and accelerate DNNs efficiently. Magnitude-based pruning schemes use the norm of filters to measure the importance, and remove the filters whose norm is lower than a given threshold [20]. There are other pruning methods using various metrics on the output features to identify and remove less important filters [14, 19, 21].

Many recent pruning methods [8, 7, 14, 24, 13] have adopted a train-prune-fine-tune strategy. This three-stage method is to train the model first, then remove the weights, and then retrain the model to restore accuracy (fine-tuning), and repeat these steps. However, performing pruning and retraining

iteratively is computationally expensive. Another commonly used strategy is to introduce the sparsity constraint of weights to the loss function in training, e.g., group Lasso and relaxed  $L_0$  regularization [27, 26, 2, 15, 23]. However, in these methods, advanced algorithms are needed to handle loss functions with non-smooth regularization in the training process or to solve additional constrained minimization problems in the pruning process.

In this paper, we propose a feature flow regularization (FFR) method, from a perspective of the evolution of feature flow, to increase the sparsity and prune filters in DNNs. Here we define the feature flow as a set of features along the network; see details in section 3.1. FFR constrains the gradient and curvature of feature flow along the network to make feature flow smoother, which controls the weights and increases the sparsity. An illustration of how FFR "smoothes" and "straightens" the feature flow is given in Figure 1; see section 3.3 for explanation. Experiments on three benchmark datasets CIFAR-10/100 [17], Tiny ImageNet [1] with VGG16 [25] and ResNet18,34,50 [11] show that FFR combined with  $L_2$  regularization significantly enhances the unstructured sparsity, channel sparsity, and filter sparsity, and accordingly prunes filters efficiently.

Our main contributions are: (1) We utilize the gradient and curvature of the feature flow to smooth evolution of features, which implicitly constrain the parameters. This method is different from the existing sparsity structure learning methods, which directly impose regularization or constraints on the parameters. Our method is also different from those pruning methods based on feature maps, which use the information of the feature map individually or in pairs (for similarity) without global relationship. (2) Simple gradient-based methods are effective to minimize the loss function with FFR combined with  $L_2$  regularization in training, e.g. stochastic gradient descent method. Compared to the regularization involving  $L_1$  norm or  $L_0$  norm, FFR is differentiable since only square of the Frobenius norm is used. (3) FFR is able to improve sparsity of DNNs significantly. The one-shot filter pruning in FFR can obtain a comparable or even better pruning ratio than that of recent state-of-the-art pruning methods on CIFAR-10 in terms of parameters and FLOPs.

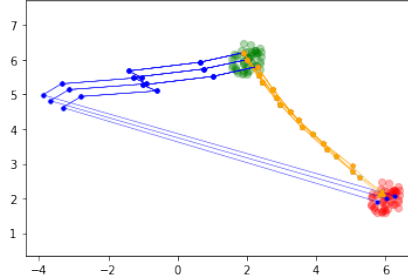


Figure 1: Feature flow visualization of five-unit ResNet without (blue) and with (orange) FFR. The green cluster consist of input data points and the red cluster contain the targets. Each curve represents the feature flow (path) along the ResNet connecting a test data pair of input and target. Along a curve, each node is an output feature of the corresponding unit in the ResNet.

## 2 Related works

**Iterative pruning.** A three-step method was proposed in [8] to prune redundant connections: train the network, prune the unimportant connections, and finally retrain the pruned network to fine tune the weights of the remaining connections. Many studies adopted this pipeline and proposed variant algorithms to improve the pruning methods. A dynamic network surgery was proposed in [7] to prune parameters effectively with reduced numbers of iterations of pruning and fine-tuning. Later, in [24, 13], pruning was formulated as a constraint optimization problem and most representative neurons were selected based on minimizing the reconstitution error. These methods are iterative on a layer by layer basis. Compared with these iterative pruning methods, our method removes filters in one pass, thereby reducing the computational cost.

**Feature-based pruning.** In addition to pruning according to the magnitude, several works studied pruning networks based on the feature information. In [14], unimportant neurons were identified based on the sparsity of the output feature maps and the network was optimized iteratively. In [19],

statistical information of feature maps was investigated to analyze the diversity and similarity, and two feature map selections were proposed for removing redundant filters. In [21], rank of feature maps was exploited and filters that generate low-rank feature maps were removed. These methods analyze the feature map alone after training. Whereas our method smooth evolution of features in the training process, therefore simplifies the pruning process.

**Structured sparsity regularization.** Some studies imposed structured sparsity regularization on weights during training to find sparse structures in one-shot instead of repeating trials. In [26], based on group Lasso, a structured sparsity learning method for structures of filters, channels, filter shapes and depth was proposed. A group sparsity regularizer was introduced in [2] that combines  $L_1$  and  $L_2$  norm on the parameters of networks. In [23], a practical method was proposed that applies  $L_0$  norm regularization to neural networks. A disadvantage of these methods is that such regularization involves  $L_0$  or  $L_1$  norm, which is non-differentiable and will hinder the use of gradient-based optimization. Thus additional optimization algorithms are needed in training in these methods. On the other hand, our FFR introduces differentiable regularization for features, and therefore does not require additional treatments in optimization.

### 3 Feature flow regularization

In this section, we apply feature flow regularization (FFR) to VGGNets and ResNets. The process can be generalized to other DNNs. In section 3.1, we present the building unit of VGGNets and ResNets, and demonstrate how we construct the feature flow. We formulate the feature flow regularization in section 3.2, and then use an example to show that FFR can effectively smooth the feature flow in section 3.3. An intuitive sparsity analysis for ResNets is given in section 3.4.

#### 3.1 Feature flow

DNNs are generally stacked by many similar building units. We define the feature flow as a set composed of the output features of each unit along the network.

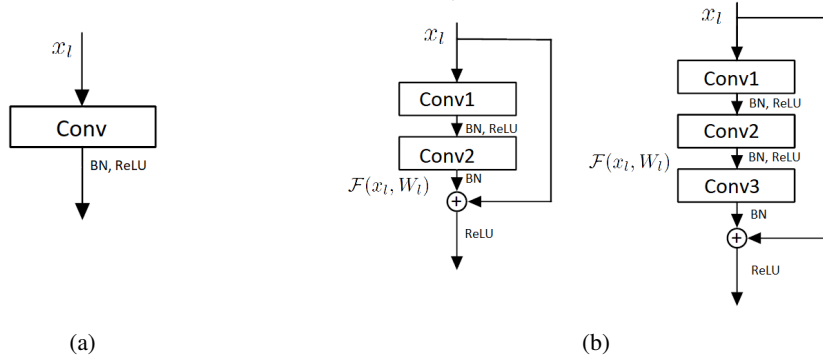


Figure 2: (a) Building unit with one convolutional layer in VGG. (b) Residual unit with two or three convolutional layers in ResNet.

**VGGNet** Convolutional networks (ConvNets [25]) are stacks of convolutional layers followed by three fully-connected layers. The building unit contains one convolutional layer, one batch normalization and one rectified linear activation function (ReLU), see Figure 2a. Given a ConvNet that consists of  $m$  convolutional layers, we can obtain the feature flow  $\{x_0, \dots, x_{m-1}\}$ . Here  $x_l$  is the output feature of the  $l + 1$ -th unit,  $l = 0, \dots, m - 1$ .

**ResNet** ResNet [11] is stacked by residual units that contain two or three convolutional layers, see Figure 2b. For the  $l$ -th residual unit, the residual function is

$$\begin{aligned}\mathcal{F}(x_l, W_l) &= W_{l,2} \otimes \sigma(\mathcal{BN}_2 \odot W_{l,1} \otimes \sigma(\mathcal{BN}_1 \odot x_l)), \text{ or} \\ \mathcal{F}(x_l, W_l) &= W_{l,3} \otimes \sigma(\mathcal{BN}_3 \odot W_{l,2} \otimes \sigma(\mathcal{BN}_2 \odot W_{l,1} \otimes \sigma(\mathcal{BN}_1 \odot x_l))),\end{aligned}$$

where  $\otimes$  denotes convolution and  $\odot$  denotes batch normalization operation. Here  $W_l = \{W_{l,k} | k = 1, \dots, K\}$  is the set of convolutional weights,  $K = 2$  or  $3$  is the number of convolutional layers in each residual unit,  $\mathcal{BN}$  is batch normalization, and  $\sigma(\cdot)$  is ReLU. Given the input feature  $x_l$ , the output feature is

$$x_{l+1} = \sigma(\mathcal{F}(x_l, W_l) + W_{s_l} x_l), \quad (1)$$

where  $W_{s_l}$  is the identity matrix if  $x_l$  and  $\mathcal{F}(x_l, W_l)$  are in the same dimension, and the learnt projection matrix otherwise. Given a ResNet that consists of  $m$  residual units, we can obtain a feature flow  $\{x_0, x_1, \dots, x_m\}$ . Here  $x_0$  is the input of the first unit and  $x_l$  is the output feature of the  $l$ -th unit,  $l = 1, \dots, m$ .

### 3.2 Feature flow regularization based on the gradient and curvature

We formulate FFR by approximating the gradient and curvature of the feature flow by finite difference formulas with two and three adjacent features, respectively. In order to control these two quantities, we add them to the loss function in training with coefficients  $k_1, k_2$ , respectively.

The formulation of FFR is as follows: for a DNN with  $B$  stages,  $m$  units, parameters  $W$ , inputs  $\{x^{(j)}, y^{(j)}\}_{j=1}^N$ , and loss function  $\frac{1}{N} \sum_{j=1}^N \mathcal{J}(x^{(j)}, y^{(j)}, W)$ ,

- Define the feature flow  $\{x_0, x_1, \dots, x_{m-1}\}^{(j)}$  (VGG) or  $\{x_0, x_1, \dots, x_m\}^{(j)}$  (ResNet) for each paired data  $(x^{(j)}, y^{(j)})$ .
- Formulate the loss function with FFR

$$\frac{1}{N} \sum_{j=1}^N \left[ \mathcal{J}(x^{(j)}, y^{(j)}, W) + k_1 \sum_{l=1}^m \|x_l^{(j)} - x_{l-1}^{(j)}\|^2 + k_2 \sum_{l=1}^{m-B} \|x_{l+1}^{(j)} - 2x_l^{(j)} + x_{l-1}^{(j)}\|^2 \right],$$

where  $\|x_l^{(j)} - x_{l-1}^{(j)}\|$  is the gradient term,  $\|x_{l+1}^{(j)} - 2x_l^{(j)} + x_{l-1}^{(j)}\|$  is the curvature term, and  $\|\cdot\|$  represents the Frobenius norm.

The adjacent states  $x_{l-1}, x_l, x_{l+1}$  may have different dimensions when the unit changes dimension. We use same strategy as [11] to fix dimension mismatch problem. For the gradient term: replace  $x_{l-1}$  by  $W_{s_l} x_{l-1}$ , where  $W_{s_l}$  is the learnt projection matrix. For the curvature term, we only restrict the curvature of  $m - B$  states, excluding the last state of each stage, and we replace  $x_{l-1}$  by  $W_{s_{l-1}} x_{l-1}$  if dimensions mismatch. The hyperparameters  $k_1, k_2$  can vary as features' dimension decreases. In our experiments, we adjust  $k_1, k_2$  to be inversely proportional to the dimension of feature.

### 3.3 Smoothing effect of FFR on the feature flow

We take a five-unit ResNet with two-dimensional features as an example to show how FFR smoothes the feature flow along the neural network, as shown in Figure 1. We use the fully-connected ResNet to learn the translation mapping from the green cluster to the red cluster. It can be seen from the figure that the evolution of features of the model trained with FFR, represented by the orange curves, is more straight than evolution of features of the model trained without FFR represented by the blue curves. This example shows that FFR can indeed effectively smooth the feature flow.

Here each residual unit in the toy ResNet contains two linear layers and outputs a two-dimensional feature. In this example, the training dataset (green and red clusters) contains 50 paired data points. The green cluster is evenly distributed in a circle with center  $(2, 6)$  and radius 0.5. The red cluster is obtained by exactly shifting the green cluster four units to the right and four units down.

### 3.4 Sparsity analysis

FFR can smooth the feature flow by controlling the gradient and curvature. Intuitively, the gradient term makes the feature flow move coherently, and the curvature term keeps the feature flow from bending too much. As a result, the residual function  $\mathcal{F}(x_l, W_l)$  in ResNet tends to have smaller magnitude and the weights are more sparse. For convenience, we ignore the projection matrix  $W_s$  in

the shortcut connection since it only appears when the stage changes. Then from Eq.(1),

$$x_{l+1} - x_l = \sigma(\mathcal{F}(x_l, W_l) + x_l) - x_l$$

$$\stackrel{\text{element-wise}}{=} \begin{cases} \mathcal{F}(x_l, W_l), & \mathcal{F}(x_l, W_l) + x_l \geq 0, \\ -x_l, & \mathcal{F}(x_l, W_l) + x_l < 0. \end{cases}$$

In the first case  $\mathcal{F}(x_l, W_l) + x_l \geq 0$ ,  $\|x_{l+1} - x_l\| = \|\mathcal{F}(x_l, W_l)\|$ . Under the hypothesis that the optimal function is closer to an identity mapping than to a zero mapping [11], the first case holds most of the time. In the second case where  $\mathcal{F}(x_l, W_l) < -x_l$ , the gradient term prefers  $x_l = \sigma(\mathcal{F}(x_{l-1}, W_{l-1}) + x_{l-1})$  to be small, which further shrinks  $\|\mathcal{F}(x_{l-1}, W_{l-1})\|$  and then encourages the first case to hold for the  $(l-1)$ -th unit.

The gradient term can enhance sparsity by pushing  $\|\mathcal{F}(x_l, W_l)\|$  to zero. Now we demonstrate this statement using a simplified example which only involves two parameters and ignoring ReLU and batch normalization. We approximate the gradient term of FFR combined with  $L_2$  regularization to

$$\sum_l (\|\mathcal{F}(x_l, W_l)\|^2 + \|W_l\|^2) = \sum_l (r_l(\omega_{l2}\omega_{l1})^2 + \omega_{l1}^2 + \omega_{l2}^2).$$

Figure 3 shows the contours of four regularization functions  $\mathcal{R}_1, \mathcal{R}_2, \mathcal{R}_3, \mathcal{R}_4$ , which are  $L_2$  regularization without FFR, FFR with coefficients  $r_l$  less than 1, FFR with coefficients  $r_l$  greater than 1, and FFR without  $L_2$  regularization respectively.

$$\mathcal{R}_1 = \omega_{l1}^2 + \omega_{l2}^2, \mathcal{R}_2 = \frac{1}{2}(\omega_{l2}\omega_{l1})^2 + \omega_{l1}^2 + \omega_{l2}^2, \mathcal{R}_3 = 2(\omega_{l2}\omega_{l1})^2 + \omega_{l1}^2 + \omega_{l2}^2, \mathcal{R}_4 = (\omega_{l2}\omega_{l1})^2.$$

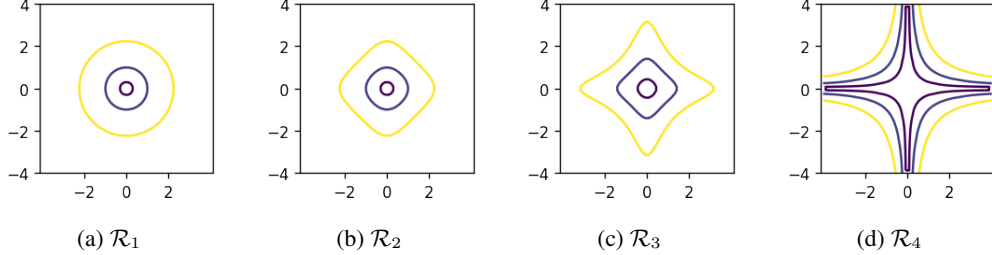


Figure 3: Contours of regularization functions:  $\mathcal{R}_1 = \omega_{l1}^2 + \omega_{l2}^2$ ,  $\mathcal{R}_2 = \frac{1}{2}(\omega_{l2}\omega_{l1})^2 + \omega_{l1}^2 + \omega_{l2}^2$ ,  $\mathcal{R}_3 = 2(\omega_{l2}\omega_{l1})^2 + \omega_{l1}^2 + \omega_{l2}^2$ ,  $\mathcal{R}_4 = (\omega_{l2}\omega_{l1})^2$ .

On the one hand, FFR combined with  $L_2$  regularization by a proper coefficient can boost sparsity while friendly to optimization. Its contours are convex and concentrate more mass in the coordinate directions (e.g.  $\mathcal{R}_2$  in Figure 3b), which are similar to the contours of  $L_1$  regularization  $|\omega_{l1}| + |\omega_{l2}|$ . However, different from non-differentiable  $L_1$  regularization, the contours do not have sharp corners. In addition, FFR can push the network to learn the most important features, an example of feature map visualization is given in Appendix A.1.  $L_1$  regularization encourages sparsity and acts as feature selector [10]. Therefore, the combination of FFR and  $L_2$  regularization can play the role of  $L_1$  regularization, and at the same time overcome the shortcoming of non-differentiation. On the other hand, FFR with coefficient greater than one combined with  $L_2$  regularization or FFR without  $L_2$  regularization have very concave contours. Non-convex constraint regions will make the optimization problem more difficult. Ablation studies in Appendix A.2 show that  $L_2$  regularization is needed together with FFR in order to achieve high accuracy and high sparsity.

## 4 Experiments

### 4.1 Implementation

We show the effectiveness of FFR by comparing two settings of models (VGG16 [25], ResNet18,34,50 [11]): one trained with FFR and the other trained without FFR. We perform experiments on CIFAR-10/100 [17] and Tiny ImageNet [1] datasets and only use RandomCrop and RandomHorizontalFlip

for preprocessing. Details of model configurations and datasets are in Appendix A.3. We initialize weights as in [12]. For CIFAR-10/100 dataset, the mini-batch size is 128. We train 200 epochs and set initial learning rate as 0.1 and divide it by 10 at the 80th, 120th, and 160th epoch. For Tiny ImageNet dataset, the mini-batch size is 50 for ResNet50 and 128 for other models. We train 60 epochs and divide initial learning rate 0.1 by 10 at the 36th, 48th, and 54th epoch. We use SGD with weight decay 0.0005 for CIFAR-10/100, 0.0001 for Tiny ImageNet, momentum 0.9. Note that  $L_2$  regularization is implemented by applying weight decay in SGD. We ran our experiments by the machine equipped with a GeForce RTX 3090 Graphics Card with 24GBs of memory. Training ResNet50 with FFR on Tiny ImageNet costs around 9 hours.

## 4.2 Sparsity

Now we explore the relation between sparsity and accuracy in the network. We consider unstructured sparsity and two types of structured sparsity: channel-level sparsity and filter-level sparsity. For a convolutional layer with parameters  $W \in R^{n \times c \times h \times \beta}$ , where  $n$  is the number of filters in the convolutional layer,  $c$  is the number of channels in each filter, and  $h, \beta$  are the height and width of each channel, respectively, we refer  $W_{:,c_i,:,:}$  as a channel and  $W_{n_i,:,:,:}$  as a filter. An illustration of channel level and filter level is given in Figure 4a. We set parameter values to zero individually or in groups based on a predefined threshold. Specifically, we select an appropriate threshold to zero out the weights so that we obtain the highest sparsity while keeping the accuracy loss less than 0.1% for CIFAR-10, 1% for CIFAR-100 and Tiny ImageNet.

**Sparsity on CIFAR-10** The hyperparameters for VGG16-FFR, ResNet18,34,50-FFR on CIFAR-10 are  $k_1 = k_2 = 2e^{-6}, 3e^{-5}, 2e^{-5}, 5e^{-6}$ , respectively. Values of sparsity that keep accuracy loss within 0.1% are shown in Table 1. In the table, unstructured sparsity is the ratio of the number of weights less than a threshold to the number of all weights. Channel/filter sparsity is the ratio of the number of channels/filters whose  $L_2$  norm are less than a threshold to the number of total channels/filters in all convolutional layers. In Figure 6, the relation of accuracy and filter sparsity is shown. More figures of unstructured sparsity and channel sparsity are in Appendix A.6. They have a similar trend to the curve of filter sparsity. The experiment results show the network trained with FFR has much higher unstructured and structured sparsity.

Particularly, Figure 4b, 4c show the exact number of zero-valued channel and filter of each convolutional layer in ResNet18 without/with FFR. Figure 5 compares the distribution of parameters of last eight convolutional layers in ResNet18 without/with FFR. Note that the parameter value range  $[-1e^{-6}, 1e^{-6}]$  of FFR is smaller than value range  $[-0.05, 0.05]$  without FFR, whereas ResNet18 with FFR still has around 40% of weights concentrating at zero in convolutional layers compared to 6% averagely in base ResNet18, indicating significantly higher sparsity by using FFR.

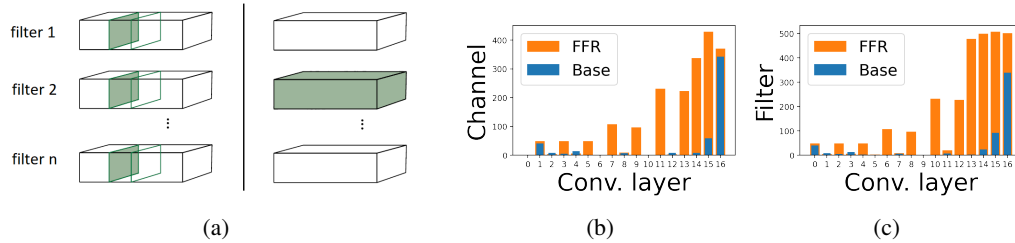


Figure 4: (a) Illustration of channel level (left) and filter level (right). (b) The number of channels zeroed out, (c) the number of filters zeroed out of each convolutional layers in ResNet18 without (blue) and with (orange) FFR. Base: without FFR.

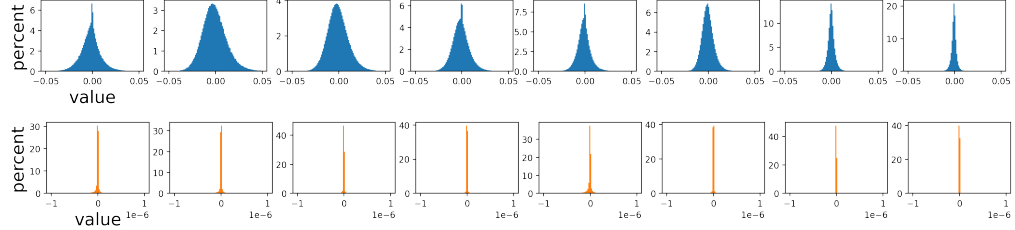


Figure 5: Histogram of weights of last eight convolutional layers in ResNet18 without (blue) and with (orange) FFR.

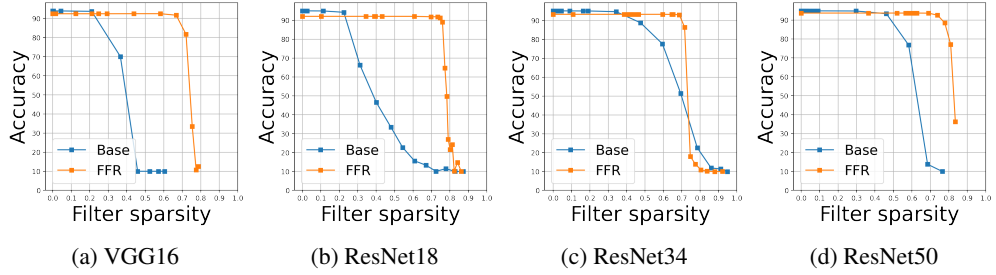


Figure 6: Relation between accuracy and filter sparsity in VGG16, ResNet18,34,50 on CIFAR-10, with FFR and without FFR. "Base" represents the results without FFR.

Table 1: Sparsity that allows accuracy to drop within 0.1%.

	Model	Un.Sparsity	Ch.Sparsity	Fil.Sparsity	Acc (%)
	VGG16-FFR	<b>0.479</b>	<b>0.557</b>	<b>0.607</b>	<b>92.48</b>
	VGG16	0.116	0.065	0.064	94
CIFAR-10	ResNet18-FFR	<b>0.821</b>	<b>0.579</b>	<b>0.728</b>	<b>92.08</b>
	ResNet18	0.055	0.146	0.140	94.96
	ResNet34-FFR	<b>0.891</b>	<b>0.657</b>	<b>0.666</b>	<b>93.29</b>
	ResNet34	0.075	0.182	0.246	95.12
	ResNet50-FFR	<b>0.505</b>	<b>0.684</b>	<b>0.698</b>	<b>93.69</b>
	ResNet50	0.055	0.183	0.315	94.85

**Sparsity on CIFAR-100** We further show the effectiveness of FFR in improving sparsity of VGG16, ResNet18,34,50 on CIFAR-100. The hyperparameters for VGG16-FFR, ResNet18,50-FFR are  $k_1 = k_2 = 2e^{-6}, 1.5e^{-5}, 1e^{-5}$  respectively and for ResNet34-FFR are  $k_1 = 1e^{-5}, k_2 = 5e^{-6}$ . Table 2 lists unstructured sparsity, channel sparsity and filter sparsity that allows accuracy to drop less than 1%. Taking VGG16 as an example, FFR improves channel sparsity and filter sparsity by around 8 and 13 times respectively while only suffering a 3.38% loss of accuracy. Figures of the relation between accuracy and sparsity are in Appendix A.7.

**Sparsity on Tiny ImageNet** Finally, we show the effectiveness of FFR in improving sparsity of Tiny ImageNet, which is a subset of a larger scale image dataset. The hyperparameters for VGG16-FFR, ResNet18,34,50-FFR on Tiny ImageNet are  $k_1 = k_2 = 1e^{-6}, 3e^{-6}, 2e^{-6}, 1.2e^{-6}$  respectively. We list values of sparsity that control accuracy drop less than 1% in Table 3. For VGG16, FFR improves channel sparsity and filter sparsity by around 80 and 235 times respectively with a 3.76% accuracy drop. For ResNet18, FFR improves channel sparsity and filter sparsity by around 9 times and accuracy is only reduced by 2.5%. Figures of the relation between accuracy and sparsity are in Appendix A.8.

Table 2: Sparsity that allows accuracy to drop within 1%.

	Model	Un.Sparsty	Ch.Sparsty	Fil.Sparsty	Acc (%)
CIFAR-100	VGG16-FFR	<b>0.645</b>	<b>0.513</b>	<b>0.476</b>	<b>71.59</b>
	VGG16	0.063	0.061	0.037	74.97
CIFAR-100	ResNet18-FFR	<b>0.291</b>	<b>0.426</b>	<b>0.378</b>	<b>74.07</b>
	ResNet18	0.028	0.049	0.051	78.04
	ResNet34-FFR	<b>0.500</b>	<b>0.411</b>	<b>0.392</b>	<b>74.57</b>
	ResNet34	0.041	0.127	0.110	77.98
	ResNet50-FFR	<b>0.371</b>	<b>0.603</b>	<b>0.562</b>	<b>73.54</b>
	ResNet50	0.036	0.189	0.332	77.85

Table 3: Sparsity that allows accuracy to drop within 1%.

	Model	Un.Sparsty	Ch.Sparsty	Fil.Sparsty	Acc (%)
Tiny ImageNet	VGG16-FFR	<b>0.058</b>	<b>0.489</b>	<b>0.469</b>	<b>56.26</b>
	VGG16	0.437	0.006	0.002	60.02
Tiny ImageNet	ResNet18-FFR	<b>0.369</b>	<b>0.338</b>	<b>0.378</b>	<b>59.04</b>
	ResNet18	0.352	0.039	0.043	61.54
	ResNet34-FFR	<b>0.468</b>	<b>0.366</b>	<b>0.396</b>	<b>61.33</b>
	ResNet34	0.238	0.108	0.104	61.85
	ResNet50-FFR	<b>0.382</b>	<b>0.593</b>	<b>0.521</b>	<b>64.49</b>
	ResNet50	0.055	0.151	0.241	65.80

### 4.3 Filter pruning

Now we use filter pruning to obtain compact networks. After some channels/filters are set as zeros by a threshold, the networks trained with FFR have many zero-value channels/filters. These zero-value channels/filters can be safely removed since they do not contribute to the output. For VGGNet, we can prune filters in any convolutional layer without limitation. For ResNet, we try two filter pruning strategies: (M1) we only prune the filters of the first layer in each residual unit. Because of the addition operation between the outputs of the shortcut and the residual unit, both outputs must have the same dimension. As a result, even if there are many zero-valued parameters, we have to retain the filters of the second layer in each residual block. (M2) we prune any convolutional layers in the residual unit and we use zeros padding for the addition operation in dimension which is pruned. This strategy enables us to prune convolutional layers in ResNet flexibly. Moreover, if all filters of the first convolutional layer are pruned, then the residual unit can be pruned. Therefore, the (M2) strategy can also prune the depth of ResNets. Our filter pruning is finished in one pass and there is no iterative pruning.

We compare filter pruning based on FFR with recent state-of-the-art pruning methods. Pruning results of VGG16 and ResNet56 on CIFAR-10 are shown in Table 4 and Table 5 respectively. In the experiment, hyperparamters of FFR are  $k_1 = k_2 = 2e^{-6}$  for VGG16, and  $k_1 = k_2 = 3e^{-6}$  for ResNet56. Here "Y", "N" indicate whether to retrain the model after pruning. We only retrain the pruned model 15 epochs if necessary.

**VGG16 on CIFAR-10** In Table 4, FFR without fine-tuning outperforms the one-shot pruning and retraining method (Li [20]). GAL [22] is a structured pruning method which uses generative adversarial learning (GAL) to solve the optimization problem for sparsity. Compared with GAL, FFR can prune more in terms of parameter and FLOPs with little lower accuracy. From the table, VGG16 pruned by FFR has around  $1.4 \times 10^6$  (vs  $2.7 \times 10^6$  by GAL-0.1) parameters left and  $1.35 \times 10^8$  (vs  $1.72 \times 10^8$  by GAL-0.1) FLOPs left with accuracy error 7.38% (vs 6.58% by GAL). Moreover, the base VGG16 of FFR has much more FLOPs because we have removed the maxpooling layer for simplicity. FFR still reduces FLOPs from  $7.96 \times 10^8$  to  $1.35 \times 10^8$  and obtains an error of 7.38%. Hence, FFR demonstrates its effectiveness in reducing parameters and FLOPs in a ConvNet with a plain structure.

**ResNet56 on CIFAR-10** In Table 5, "FFR-pruned" denotes (M1) and "FFR-pruned-Z" denotes (M2). Compared with He [13] with a 8.2% error after fine-tuning, our FFR reduces more FLOPs (57.5% pruned vs 50.6% pruned by He [13]) while with better result of 7.79% error. These results show that FFR can also prune filters effectively in ResNet.

Table 4: Pruning results of VGG16 on CIFAR-10.

Model	Param.	Param. Pruned	FLOPs	FLOPs Pruned	Error(%)	Fine-tune
FFR-base	$1.5 \times 10^7$		$7.96 \times 10^8$		7.52	
FFR-pruned	$2.5 \times 10^6$	<b>83.3%</b>	$1.75 \times 10^8$	<b>78.0%</b>	7.78	N
FFR-pruned	$1.4 \times 10^6$	<b>90.7%</b>	$1.35 \times 10^8$	<b>83.0%</b>	9.94 / 7.38	N / Y
base	$1.5 \times 10^7$		$3.13 \times 10^8$		6.75	
Li[20]-pruned	$5.4 \times 10^6$	64.0%	$2.06 \times 10^8$	34.2%	6.60	Y
SSS[15]	$3.9 \times 10^6$	73.8%	$1.83 \times 10^8$	41.6%	6.98	N
GAL-0.1[22]	$2.7 \times 10^6$	82.2%	$1.72 \times 10^8$	45.2%	9.22 / 6.58	N / Y
Hrank[21]	$2.6 \times 10^6$	82.1%	$1.09 \times 10^8$	65.3%	7.66	Y

Table 5: Pruning results of ResNet56 on CIFAR-10. FFR-pruned-Z represents "zero padding" pruning strategy.

Model	Param.	Param. Pruned	FLOPs	FLOPs Pruned	Error(%)	Fine-tune
FFR-base	$8.6 \times 10^5$		$1.26 \times 10^8$		7.57	
FFR-pruned	$7.5 \times 10^5$	<b>12.7%</b>	$9.59 \times 10^7$	<b>23.3%</b>	7.96	N
FFR-pruned-Z	$5.9 \times 10^5$	<b>31.1%</b>	$7.56 \times 10^7$	<b>39.9%</b>	8.76	N
FFR-pruned-Z	$5.2 \times 10^5$	<b>38.7%</b>	$6.88 \times 10^7$	<b>45.3%</b>	9.59	N
FFR-pruned-Z	$4.6 \times 10^5$	<b>46.3%</b>	$5.35 \times 10^7$	<b>57.5%</b>	20.64 / 7.79	N / Y
base	$8.5 \times 10^5$		$1.25 \times 10^8$		6.96	
Li[20]-pruned-B	$7.3 \times 10^5$	13.7%	$9.09 \times 10^7$	27.6%	6.94	Y
He[13]	-	-	$6.20 \times 10^7$	50.6%	9.20 / 8.20	N / Y
GAL-0.6 [22]	$7.5 \times 10^5$	11.8%	$7.83 \times 10^7$	37.6%	7.02 / 6.62	N / Y
Hrank[21]	$4.9 \times 10^5$	42.4%	$6.27 \times 10^7$	50.0%	6.83	Y

## 5 Limitation and discussion

Since in FFR, the regularization is imposed on features, a limitation of this method is that we are not able to predetermine the sparsity, although experimental results using FFR have shown significant sparsity improvement. In order to balance sparsity and accuracy, we need to tune the hyperparameters  $k_1, k_2$ , which vary with networks and datasets. In addition, FFR achieves high sparsity at the cost of a slight loss in accuracy compared with a network trained without FFR. This is reasonable because the FFR term is directly added to the loss function. The accuracy can be further increased by combining FFR with other methods in the pruning process.

We do not think our method has any potential negative social impact or ethical problem.

## 6 Conclusion

In this paper, we propose a simple and effective regularization method (FFR) from a new perspective of the evolution of features. FFR smoothes the evolution of features by imposing controls on the gradient and curvature of the feature flow, leading to significant increase of sparsity in DNNs. We perform a sparsity analysis of FFR for ResNet in a simplified case to validate the effectiveness of this method. By considering contours of the FFR term, we find that FFR can play a similar role as that of  $L_1$  regularization in encouraging sparsity, while remaining differentiable and friendly

to training. Moreover, feature maps visualization shows that FFR can select features. That is, only important features are learnt. Experimental results show that FFR can significantly enhance unstructured sparsity, channel sparsity, filter sparsity, and therefore we can prune filters efficiently in one pass. Future work may include: (1) perform rigorous sparsity analysis for FFR, and (2) integrate FFR with other pruning methods to achieve better pruning results.

## Acknowledgments

This work was supported by Hong Kong University of Science and Technology grant IEG19SC04 and HKUST Shenzhen Research Institute grant P2070.

## References

- [1] URL <https://www.image-net.org/>.
- [2] Jose M Alvarez and Mathieu Salzmann. Learning the number of neurons in deep networks. In D. Lee, M. Sugiyama, U. Luxburg, I. Guyon, and R. Garnett, editors, *Advances in Neural Information Processing Systems*, volume 29. Curran Associates, Inc., 2016. URL <https://proceedings.neurips.cc/paper/2016/file/6e7d2da6d3953058db75714ac400b584-Paper.pdf>.
- [3] Baoyuan Liu, Min Wang, H. Foroosh, M. Tappen, and M. Penksy. Sparse convolutional neural networks. In *2015 IEEE Conference on Computer Vision and Pattern Recognition (CVPR)*, pages 806–814, 2015. doi: 10.1109/CVPR.2015.7298681.
- [4] Misha Denil, Babak Shakibi, Laurent Dinh, Marc’Aurelio Ranzato, and Nando de Freitas. Predicting parameters in deep learning. 2013. URL <http://arxiv.org/abs/1306.0543>.
- [5] Emily Denton, Wojciech Zaremba, Joan Bruna, Yann LeCun, and Rob Fergus. Exploiting linear structure within convolutional networks for efficient evaluation. 2014. URL <http://arxiv.org/abs/1404.0736>.
- [6] Yunchao Gong, Liu Liu, Ming Yang, and Lubomir D. Bourdev. Compressing deep convolutional networks using vector quantization. 2014. URL <http://arxiv.org/abs/1412.6115>.
- [7] Yiwen Guo, Anbang Yao, and Yurong Chen. Dynamic network surgery for efficient dnns. 2016. URL <http://arxiv.org/abs/1608.04493>.
- [8] Song Han, Jeff Pool, John Tran, and William J. Dally. Learning both weights and connections for efficient neural networks. 2015. URL <http://arxiv.org/abs/1506.02626>.
- [9] Babak Hassibi and David Stork. Second order derivatives for network pruning: Optimal brain surgeon. In S. Hanson, J. Cowan, and C. Giles, editors, *Advances in Neural Information Processing Systems*, volume 5. Morgan-Kaufmann, 1993. URL <https://proceedings.neurips.cc/paper/1992/file/303ed4c69846ab36c2904d3ba8573050-Paper.pdf>.
- [10] T. Hastie, R. Tibshirani, and J.H. Friedman. *The Elements of Statistical Learning: Data Mining, Inference, and Prediction*. Springer series in statistics. Springer, 2009. ISBN 9780387848846. URL <https://books.google.com.hk/books?id=eBSgoAEACAAJ>.
- [11] Kaiming He, Xiangyu Zhang, Shaoqing Ren, and Jian Sun. Deep residual learning for image recognition. 2015. URL <http://arxiv.org/abs/1512.03385>.
- [12] Kaiming He, Xiangyu Zhang, Shaoqing Ren, and Jian Sun. Delving deep into rectifiers: Surpassing human-level performance on imagenet classification. 2015. URL <http://arxiv.org/abs/1502.01852>.
- [13] Yihui He, Xiangyu Zhang, and Jian Sun. Channel pruning for accelerating very deep neural networks. 2017. URL <http://arxiv.org/abs/1707.06168>.
- [14] Hengyuan Hu, Rui Peng, Yu-Wing Tai, and Chi-Keung Tang. Network trimming: A data-driven neuron pruning approach towards efficient deep architectures. 2016. URL <http://arxiv.org/abs/1607.03250>.

- [15] Zehao Huang and Naiyan Wang. Data-driven sparse structure selection for deep neural networks. 2017. URL <http://arxiv.org/abs/1707.01213>.
- [16] Max Jaderberg, Andrea Vedaldi, and Andrew Zisserman. Speeding up convolutional neural networks with low rank expansions. 2014. URL <http://arxiv.org/abs/1405.3866>.
- [17] A. Krizhevsky and G. Hinton. Learning multiple layers of features from tiny images. *Master's thesis, Department of Computer Science, University of Toronto*, 2009.
- [18] Yann LeCun, John Denker, and Sara Solla. Optimal brain damage. In D. Touretzky, editor, *Advances in Neural Information Processing Systems*, volume 2. Morgan-Kaufmann, 1990. URL <https://proceedings.neurips.cc/paper/1989/file/6c9882bbac1c7093bd25041881277658-Paper.pdf>.
- [19] Hang Li, Chen Ma, Wei Xu, and Xue Liu. Feature statistics guided efficient filter pruning. 2020. URL <https://arxiv.org/abs/2005.12193>.
- [20] Hao Li, Asim Kadav, Igor Durdanovic, Hanan Samet, and Hans Peter Graf. Pruning filters for efficient convnets. 2016. URL <http://arxiv.org/abs/1608.08710>.
- [21] Mingbao Lin, Rongrong Ji, Yan Wang, Yichen Zhang, Baochang Zhang, Yonghong Tian, and Ling Shao. Hrank: Filter pruning using high-rank feature map, 2020.
- [22] Shaohui Lin, Rongrong Ji, Chenqian Yan, Baochang Zhang, Liujuan Cao, Qixiang Ye, Feiyue Huang, and David S. Doermann. Towards optimal structured CNN pruning via generative adversarial learning. 2019. URL <http://arxiv.org/abs/1903.09291>.
- [23] Christos Louizos, Max Welling, and Diederik P. Kingma. Learning sparse neural networks through  $l_0$  regularization, 2018.
- [24] Jian-Hao Luo, Jianxin Wu, and Weiyao Lin. Thinet: A filter level pruning method for deep neural network compression. 2017. URL <http://arxiv.org/abs/1707.06342>.
- [25] Karen Simonyan and Andrew Zisserman. Very deep convolutional networks for large-scale image recognition. In Yoshua Bengio and Yann LeCun, editors, *3rd International Conference on Learning Representations, ICLR 2015, San Diego, CA, USA, May 7-9, 2015, Conference Track Proceedings*, 2015. URL <http://arxiv.org/abs/1409.1556>.
- [26] Wei Wen, Chunpeng Wu, Yandan Wang, Yiran Chen, and Hai Li. Learning structured sparsity in deep neural networks. 2016. URL <http://arxiv.org/abs/1608.03665>.
- [27] Hao Zhou, Jose M. Alvarez, and Fatih Porikli. Less is more: Towards compact cnns. In Bastian Leibe, Jiri Matas, Nicu Sebe, and Max Welling, editors, *Computer Vision - ECCV 2016 - 14th European Conference, Amsterdam, The Netherlands, October 11-14, 2016, Proceedings, Part IV*, volume 9908 of *Lecture Notes in Computer Science*, pages 662–677. Springer, 2016. doi: 10.1007/978-3-319-46493-0\_40. URL [https://doi.org/10.1007/978-3-319-46493-0\\_40](https://doi.org/10.1007/978-3-319-46493-0_40).

## A Appendix

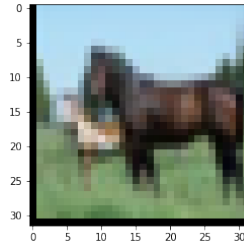
### A.1 Feature maps visualization

In order to further demonstrate that FFR can push the network to learn the most important features mentioned in section 3.4 of the main text, we visualize the feature maps of the first convolutional layer in ResNet34 with/without FFR on CIFAR-10, and the results are shown in Figures 7 and 8. From these figures, we observe that for features maps of ResNet34 with FFR, most of them contain no information (black squares) and only a few (around 10 out of 64) contain important information. The corresponding filters of feature maps with no information can be removed. Therefore FFR allows us to prune more filters. Whereas ResNet34 without FFR has less feature maps without information, and more blurry feature maps which may be less informative but may not be removed. Similar properties are also observed in feature maps of other input images of ResNet34. This shows that FFR can select more important features, which enables us to prune more filters.

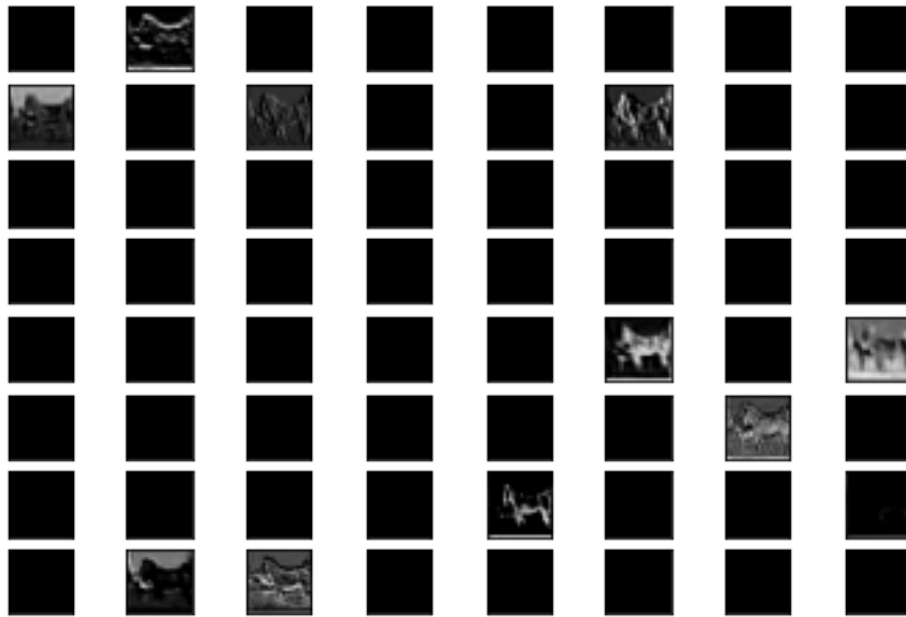
### A.2 Ablation study

In this subsection, we study the effect of hyperparameters  $k_1, k_2$  in feature flow regularization (FFR) on the relation of sparsity and accuracy. The relation curves of ResNet18 on CIFAR-100 are shown in Figure 9. In the figure, unstructured sparsity is the ratio of the number of weights less than a threshold to the number of all weights. Channel/filter sparsity is the ratio of the number of channels/filters whose  $L_2$  norm are less than a threshold to the number of total channels/filters in all convolutional layers. We use increasing thresholds to zero the weights individually or in channels/filters, then we obtain the corresponding accuracy and plot curves.

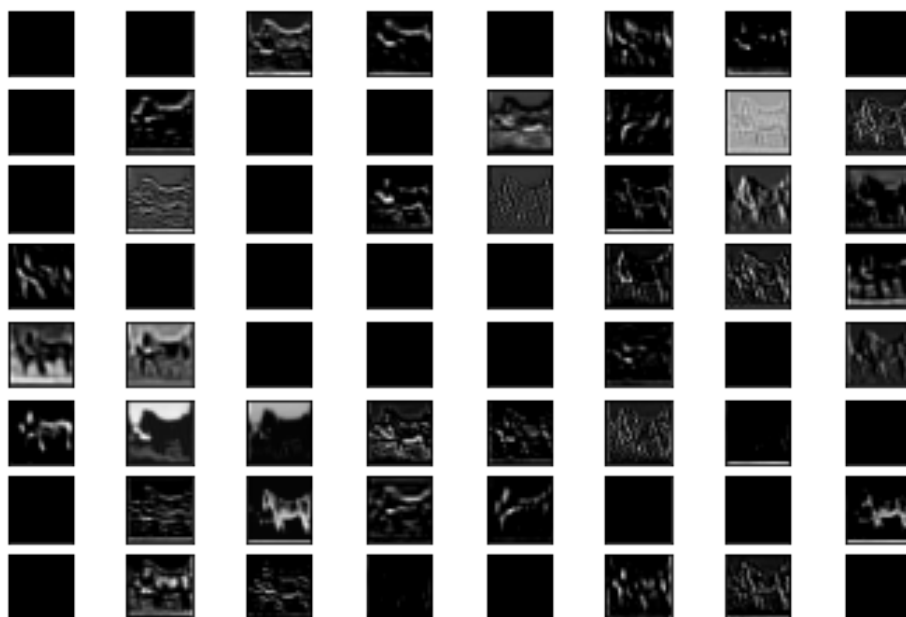
From Figure 9, FFR with greater  $k_1, k_2$  brings higher sparsity and at the same time suffers lower accuracy. This is a trade-off between sparsity and accuracy. We can also see that  $L_2$  regularization is needed together with FFR in order to achieve high accuracy and high sparsity, as pointed out in section 3.4 of the main text.



(a) Input: No.12 figure from CIFAR-10. Class: horse.

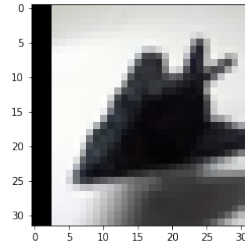


(b) Feature maps of ResNet34 with FFR.

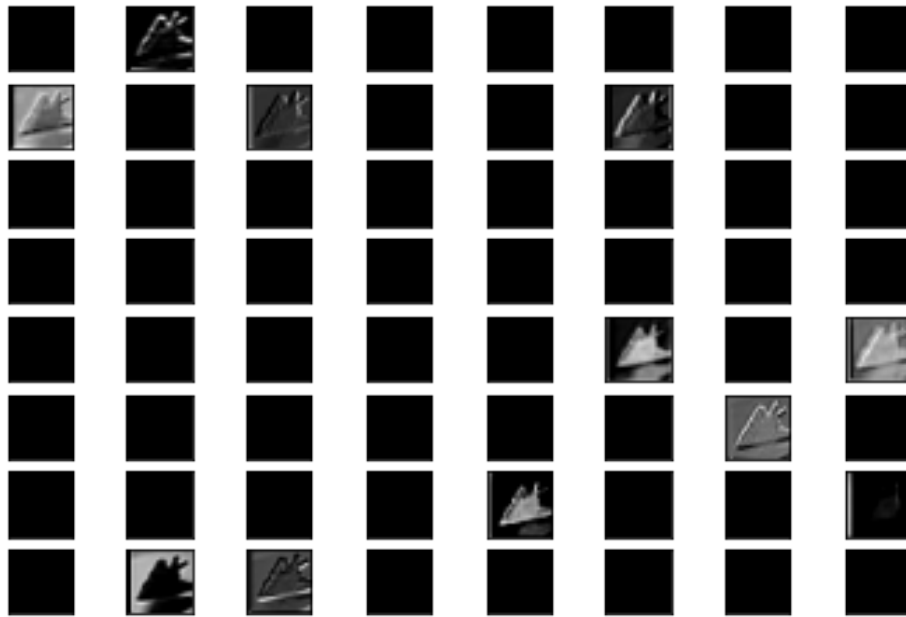


(c) Feature maps of ResNet34 without FFR.

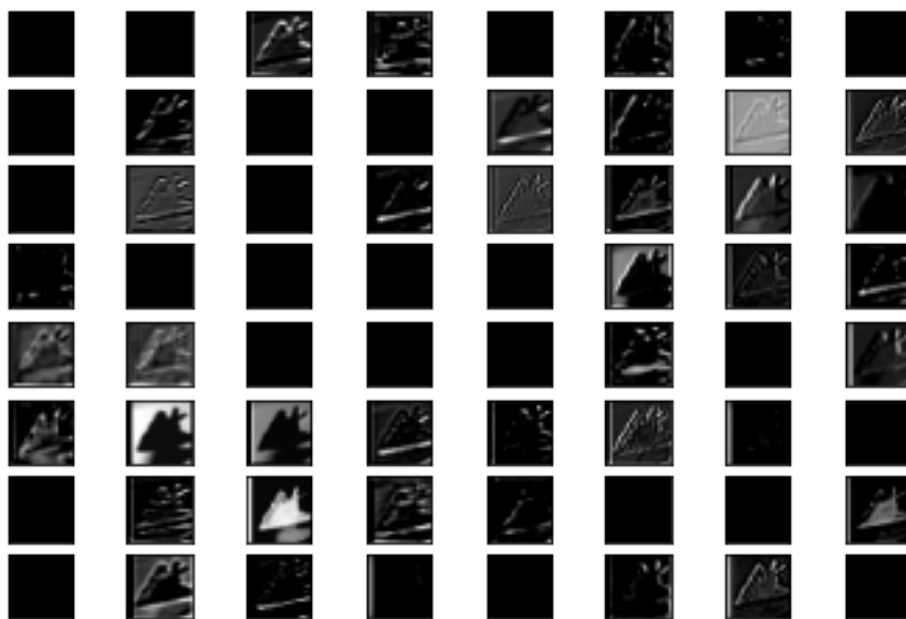
Figure 7: Feature maps of the first convolutional layer in ResNet34 with/without FFR.



(a) Input: No.29 figure from CIFAR-10. Class: airplane.



(b) Feature maps of ResNet34 with FFR.



(c) Feature maps of ResNet34 without FFR.

Figure 8: Feature maps of the first convolutional layer in ResNet34 with/without FFR.

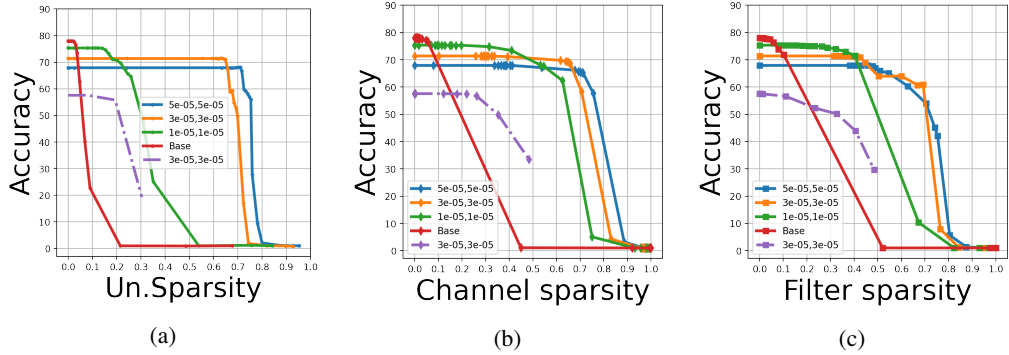


Figure 9: (a) Unstructured sparsity-accuracy curves, (b) Channel sparsity-accuracy curves, (c) Filter sparsity-accuracy curves. Five curves represent ResNet-18 with FFR coefficients pairs  $k_1 = k_2 = 5e^{-5}$  (blue line),  $k_1 = k_2 = 3e^{-5}$  (orange line),  $k_1 = k_2 = 1e^{-5}$  (green line), ResNet-18 without FFR (Base, i.e.,  $k_1 = k_2 = 0$ , red line), and ResNet-18 with FFR and without  $L_2$  regularization (purple dashed-dot line,  $k_1 = k_2 = 3e^{-5}$ ) on CIFAR-100, respectively. The numbers in the figure are the values of hyperparameters  $k_1, k_2$ .

### A.3 Models and Datasets

For the experiments in section 4, we provide details of VGG16, ResNet18,34,50 and CIFAR10/100, Tiny ImageNet datasets in Table 6 and Table 7, respectively.

Table 6: Model configuration.

Model	VGG-16	ResNet-18	ResNet-34	ResNet-50	
conv. layers	13	17	33	49	
conv. types		$[3 \times 3, 64] \times 1$ , $[3 \times 3, 64] \times 2$ , $[3 \times 3, 128] \times 2$ , $[3 \times 3, 256] \times 3$ , $[3 \times 3, 512] \times 6$ .	$[3 \times 3, 64] \times 1$ , $[3 \times 3, 64] \times 2$ , $[3 \times 3, 128] \times 2$ , $[3 \times 3, 256] \times 2$ , $[3 \times 3, 512] \times 2$ .	$[3 \times 3, 64] \times 1$ , $[3 \times 3, 64] \times 3$ , $[3 \times 3, 128] \times 4$ , $[3 \times 3, 256] \times 6$ , $[3 \times 3, 512] \times 3$ .	$[3 \times 3, 64] \times 1$ , $[3 \times 3, 64] \times 3$ , $[1 \times 1, 128] \times 4$ , $[1 \times 1, 256] \times 6$ , $[1 \times 1, 512] \times 3$ , $[1 \times 1, 1024] \times 6$ , $[1 \times 1, 2048] \times 3$ .
states in feature flow	13	9	17	17	
stages	4	4	4	4	

Table 7: Datasets

Dataset	Classes	Training Images	Testing Images	Image Size
CIFAR-10	10	50K	10K	32 × 32
CIFAR-100	100	50K	10K	32 × 32
Tiny ImageNet	200	100K	10K	64 × 64

As an example, here we give the feature flow and the FFR term of ResNet18. ResNet18 has 4 stages, 8 residual units:

$$\begin{bmatrix} 3 \times 3, & 64 \\ 3 \times 3, & 64 \end{bmatrix} \times 2, \begin{bmatrix} 3 \times 3, & 128 \\ 3 \times 3, & 128 \end{bmatrix} \times 2, \begin{bmatrix} 3 \times 3, & 256 \\ 3 \times 3, & 256 \end{bmatrix} \times 2, \begin{bmatrix} 3 \times 3, & 512 \\ 3 \times 3, & 512 \end{bmatrix} \times 2.$$

The feature flow is  $\{x_0, x_1, \dots, x_8\}$ , where  $x_0$  is the output feature of the first convolutional layers, and  $x_l$  is the output feature of the  $l$ -th residual unit,  $l = 1, \dots, 8$ .

The expression of FFR term (omitting superscript) is

$$\begin{aligned} & k_1(\|x_1 - x_0\|^2 + \|x_2 - x_1\|^2) + 4k_1(\|x_3 - W_{s_2}x_2\|^2 + \|x_4 - x_3\|^2) \\ & + 16k_1(\|x_5 - W_{s_4}x_4\|^2 + \|x_6 - x_5\|^2) + 64k_1(\|x_7 - W_{s_6}x_6\|^2 + \|x_8 - x_7\|^2) \\ & + k_2\|x_2 - 2x_1 + x_0\|^2 + 4k_2\|x_4 - 2x_3 + W_{s_2}x_2\|^2 \\ & + 16k_2\|x_6 - 2x_5 + W_{s_4}x_4\|^2 + 64k_2\|x_8 - 2x_7 + W_{s_6}x_6\|^2. \end{aligned}$$

This FFR term is included in the loss function. Note that the dimension of the feature shrinks by a quarter as the type of residual unit changes. Hence we quadruple  $k_1, k_2$  correspondingly.

#### A.4 Histogram of parameters in convolutional layers

In section 4.2, we show the histogram of weights of last eight convolutional layers in ResNet18 without/with FFR on CIFAR-10. In Figure 10, we show the histogram of weights of more convolutional layers. These figures show that network trained with FFR has much higher unstructured sparsity.

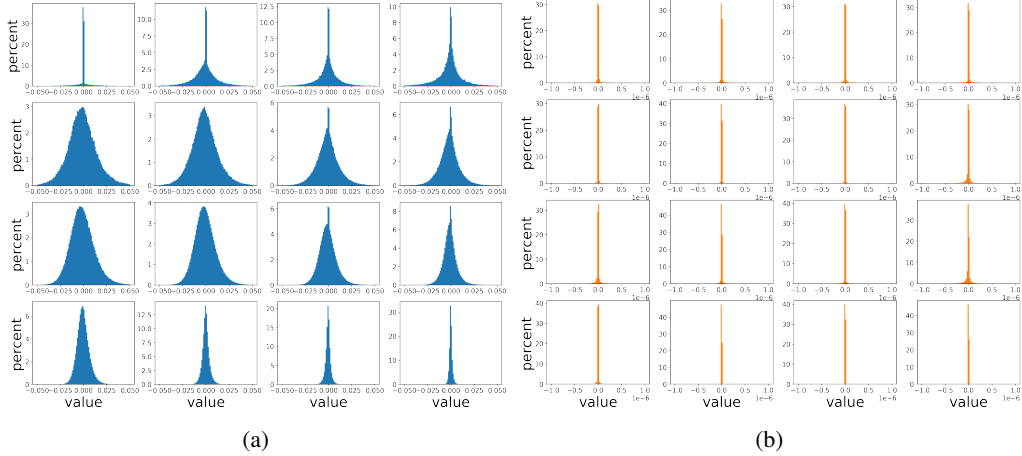


Figure 10: Histogram of weights of last sixteen convolutional layers in ResNet18 without (blue) and with (orange) FFR on CIFAR-10.

#### A.5 The number of channels and filters zeroed out of each layer

In section 4.2, we compare the number of channels and filters zeroed out in ResNet18 on CIFAR-10. Here we compare the number of channels and filters zeroed out (accuracy drop within 1%) of each convolutional layer in ResNet18 and ResNet50 on Tiny ImageNet in Figure 11 and Figure 12, respectively. These figures show that network trained with FFR has much higher channel/filter sparsity.

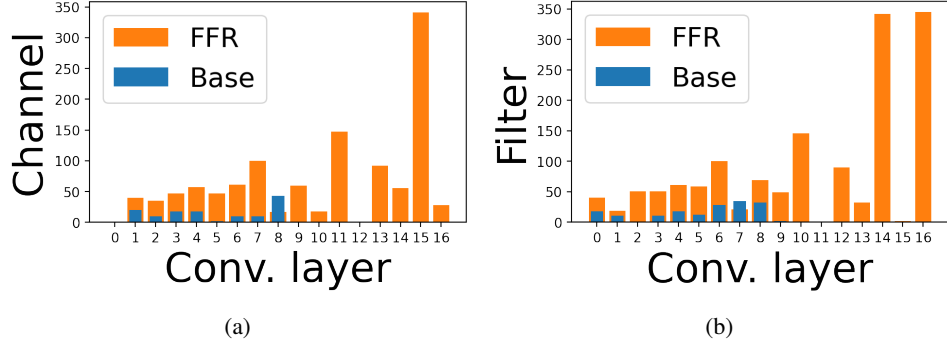


Figure 11: (a) The number of channels zeroed out, and (b) the number of filters zeroed out of each convolutional layers in ResNet18 without (blue) and with (orange) FFR on Tiny ImageNet. Base: without FFR.

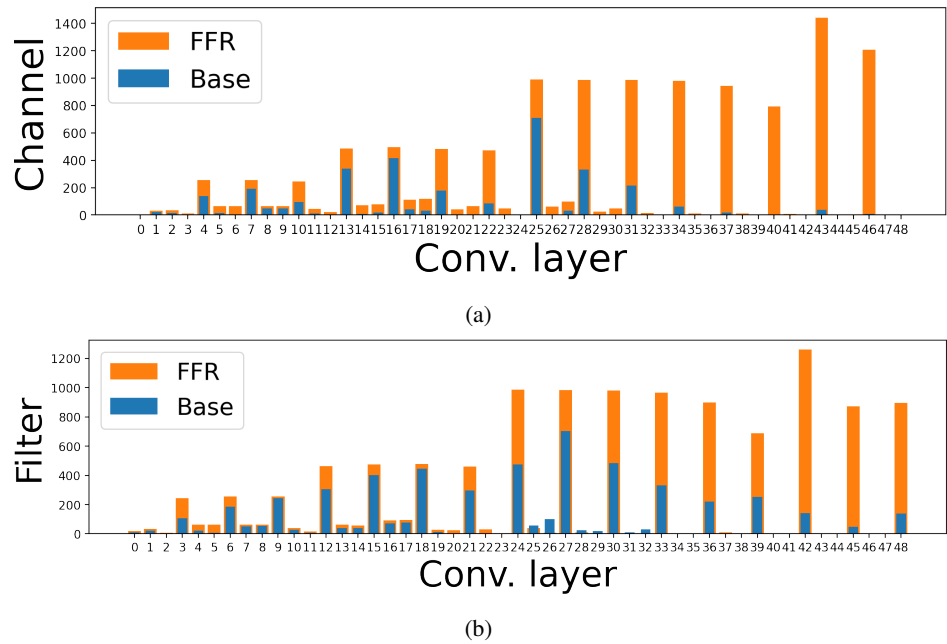


Figure 12: (a) The number of channels zeroed out, and (b) the number of filters zeroed out of each convolutional layers in ResNet50 without (blue) and with (orange) FFR on Tiny ImageNet. Base: without FFR.

## A.6 Sparsity on CIFAR-10

The relations of accuracy and unstructured sparsity, channel sparsity, filter sparsity of VGG16, ResNet18,34,50 on CIFAR-10 are shown in Figure 13. This provides more details for Table 1 in section 4.2. The comparisons show that the network trained with FFR has much higher unstructured and structured sparsity. Section A.7 and A.8 on CIFAR-100 and Tiny ImageNet give the same conclusion.

## A.7 Sparsity on CIFAR-100

The relations of accuracy and unstructured sparsity, channel sparsity, filter sparsity of VGG16, ResNet18,34,50 on CIFAR-100 are shown in Figure 14. This provides more details for Table 2 in section 4.2.

## A.8 Sparsity on Tiny ImageNet

The relations of accuracy and unstructured sparsity, channel sparsity, filter sparsity of VGG16, ResNet18,34,50 on Tiny ImageNet are shown in Figure 15. This provides more details for Table 3 in section 4.2.

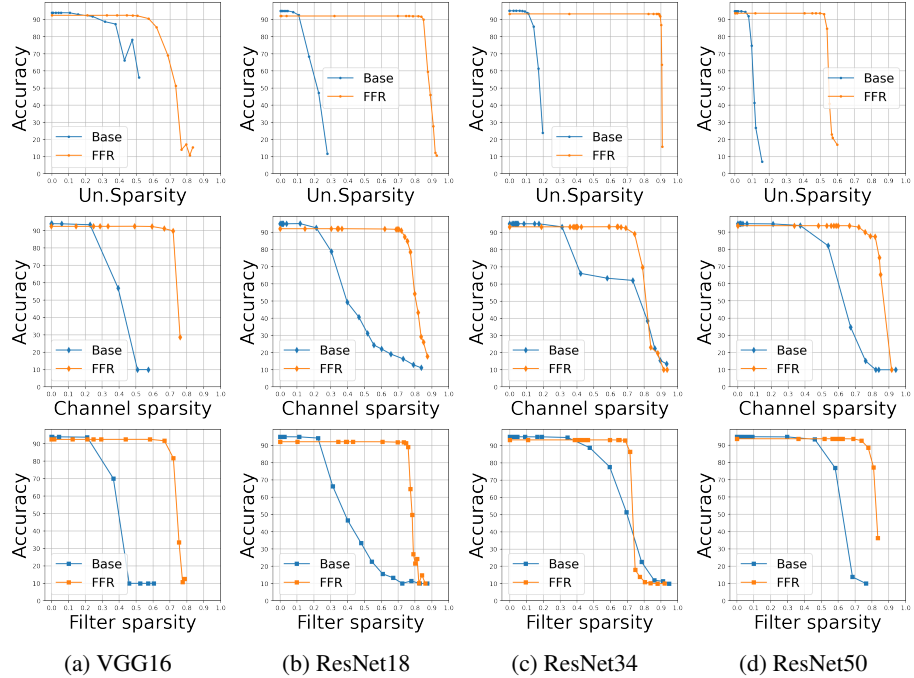
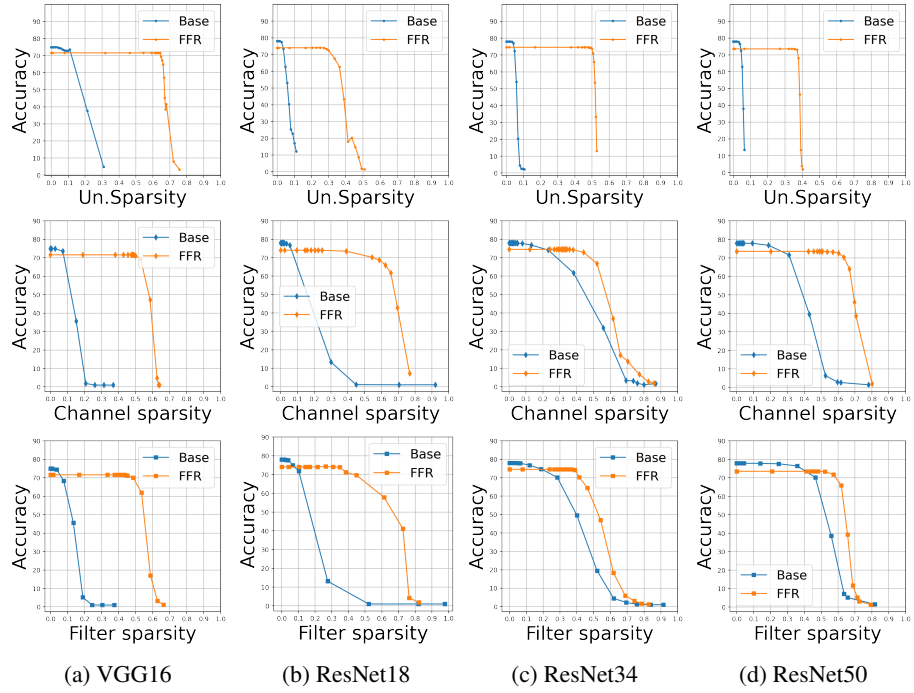


Figure 13: Relation between accuracy and unstructured sparsity, channel sparsity, filter sparsity in VGG16, ResNet18,34,50 on CIFAR-10, with FFR and without FFR. Base: without FFR.



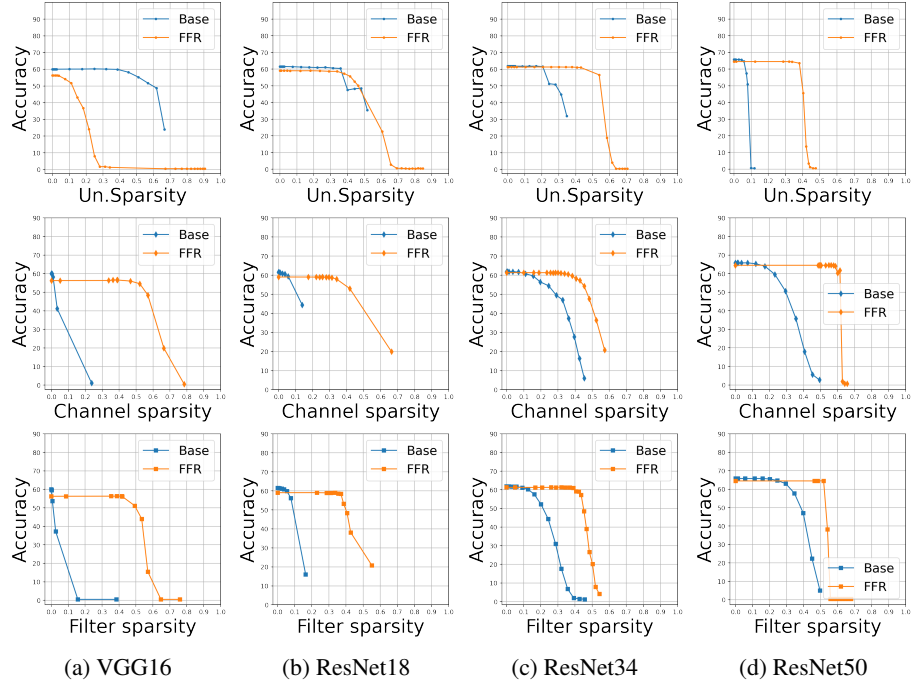
(a) VGG16

(b) ResNet18

(c) ResNet34

(d) ResNet50

Figure 14: Relation between accuracy and unstructured sparsity, channel sparsity, filter sparsity in VGG16, ResNet18,34,50 on CIFAR-100, with FFR and without FFR. Base: without FFR.



(a) VGG16

(b) ResNet18

(c) ResNet34

(d) ResNet50

Figure 15: Relation between accuracy and unstructured sparsity, channel sparsity, filter sparsity in VGG16, ResNet18,34,50 on Tiny ImageNet, with FFR and without FFR. Base: without FFR.

### A.9 Error bars of sparsity and accuracy

We report error bars of unstructured sparsity, channel sparsity, filter sparsity and accuracy in bar plots, see Figure 16. We run the experiments five times under the following setting: VGG16 with FFR coefficients  $k_1 = k_2 = 2e^{-6}$  on CIFAR-10. In the figure, the height of the bars is the mean of each group and the height of the error bars is twice of the standard deviation of each group.

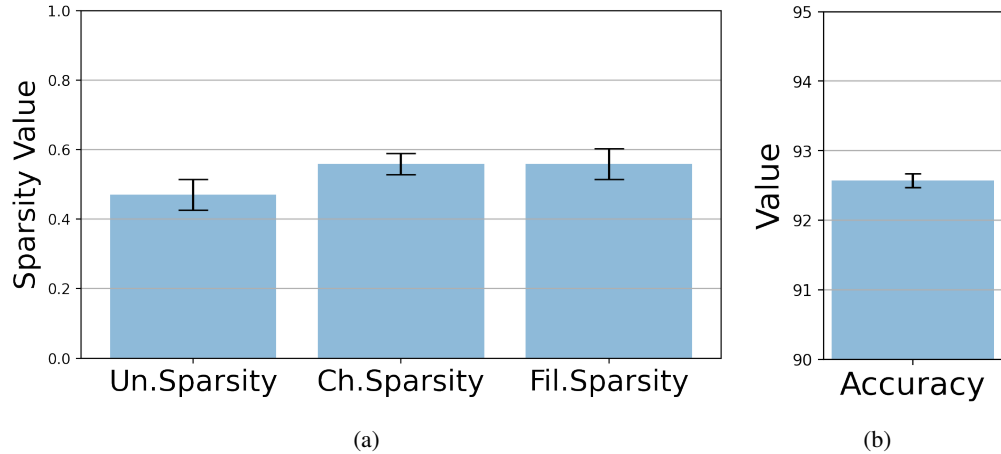


Figure 16: Error bars of (a) sparsity and (b) accuracy of VGG16 on CIFAR-10.